PHYSICAL REVIEW C **88**, 024601 (2013)

Quantum interference effects in an ensemble of ^{229}Th nuclei interacting with coherent light

Sumanta Das,* Adriana Pálffy,† and Christoph H. Keitel‡
Max-Planck-Institut für Kernphysik, Saupfercheckweg 1, D-69117 Heidelberg, Germany
(Received 26 May 2013; published 2 August 2013)

As a unique feature, the ^{229}Th nucleus has an isomeric transition in the vacuum ultraviolet that can be accessed by optical lasers. The interference effects occurring in the interaction between coherent optical light and an ensemble of ^{229}Th nuclei are investigated theoretically. We consider the scenario of nuclei doped in vacuum ultraviolet transparent crystals and take into account the effect of different doping sites and therefore different lattice fields that broaden the nuclear transition width. This effect is shown to come into interplay with interference effects due to the hyperfine splitting of the ground and isomeric nuclear states. We investigate possible experimentally available situations involving two-, three- and four-level schemes of quadrupole sublevels of the ground and isomeric nuclear states coupling to one or two coherent fields. Specific configurations which offer clear signatures of the isomer excitation advantageous for the more precise experimental determination of the transition energy are identified. Furthermore, it is shown that population trapping into the isomeric state can be achieved. This paves the way for further nuclear quantum optics applications with ^{229}Th such as nuclear coherent control.

DOI: 10.1103/PhysRevC.88.024601 PACS number(s): 23.20.Lv, 42.50.Gy, 82.80.Ej

I. INTRODUCTION

Out of the entire nuclear chart, ^{229}Th has the so far only known nuclear transition that can be accessed with available optical lasers. The transition energy is at present estimated to be 7.8 ± 0.5 eV [1], corresponding to the vacuum-ultraviolet (VUV) range. Except for this unique example, direct laser driving of nuclear transitions has been so far discussed in the context of the commissioning of x-ray light sources such as the x-ray free electron laser (XFEL) [2–4]. In both cases, the interest in nuclear quantum optics applications is fueled by the expected parallel to intriguing and counterintuitive quantum interference effects in multilevel atomic and molecular systems [5,6]. Induced atomic and molecular coherences are related to many optical phenomena such as enhanced nonlinear effects [7], electromagnetically induced transparency (EIT) [8,9], coherent population trapping [10], stimulated Raman adiabatic passage (STIRAP) [11], lasing without inversion [12,13], efficient nonlinear frequency conversions [14], collective quantum dynamics [15–17], and vacuum induced coherence in photoassociation [18], to name a few. The possibility of similar coherent control in nuclear systems, also related to specific nuclear incentives as isomer depletion or a nuclear γ-ray laser, have been considered with great interest [2,3,19,20]. All these quantum optical effects require strong Rabi coupling of the driving field to the considered transitions [5,6]. Consequently it is important to achieve direct laser driving of nuclear transitions if similar phenomena in nuclei are to be observed experimentally.

However, the direct interaction of laser fields with nuclei is generally difficult to achieve due to (a) small nucleus-laser interaction matrix elements [21], (b) ineffective nuclear polarization, as the populations of the hyperfine levels are usually nearly equal even at very low temperatures, and (c) the mostly high nuclear excitation energies in the keV to MeV range which are still out of reach for currently available coherent light sources. In this regard, the isomeric transition ($I_{is}^{\pi} = 3/2^+) \rightarrow (I_g^{\pi} = 5/2^+)$ (see Fig. 1) of ^{229}Th is the notable exception. This transition is currently a strong candidate for frequency metrology [22,23] and is in focus for several other potential applications such as temporal variation of the fine structure constant [24], building a nuclear laser in the optical range [25], or providing an exciting platform for nuclear quantum optics and coherent control of VUV photons [2,4,26–29].

Even with energies in the VUV range it is difficult to investigate field-induced coherence effects among the hyperfine levels of this ^{229}Th isomeric transition by direct laser coupling at present. This is primarily due to an 1 eV uncertainty in the transition energy and a very narrow radiative transition width of $\sim$0.1 mHz. A correspondingly narrow bandwidth VUV laser source is at present available only within limitations and could not be directly employed prior to attaining better knowledge of the transition frequency. A viable alternative to attain optical probing of the isomeric transition is to use coherent light scattering off nuclei in the low-excitation limit [30–35] by a broadband source such as a synchrotron or available VUV lasers. In particular, enhanced transient fluorescence in the forward direction obtained in such scattering was found to be useful in search for the isomeric transition frequency of ^{229}Th nuclei [36]. Coherence and interference effects are expected to help both in the precise determination of the isomeric transition and in developing a platform for nuclear quantum optics studies based on the isomeric transition of ^{229}Th.

In Ref. [36] a first step in this direction was made by investigating a novel scheme for the direct measurement of the transition energy via electromagnetically modified nuclear forward scattering (NFS) involving two fields that couple to

*sumanta.das@mpi-hd.mpg.de
†palffy@mpi-hd.mpg.de
‡keitel@mpi-hd.mpg.de

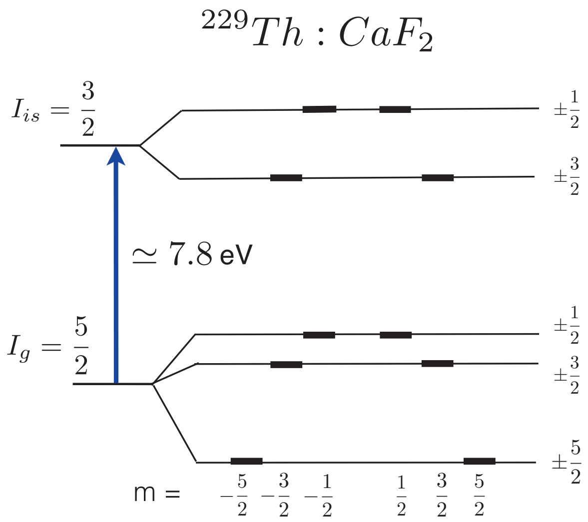

FIG. 1. (Color online) Quadrupole splitting of ^{229}Th doped in VUV-transparent crystals such as $LiCaAlF_6$ or CaF_2. Here m is the magnetic quantum number. The splittings are on the order of MHz [23].

three nuclear states. This scheme provides an unmistakable signature of the isomeric fluorescence in nuclear spectroscopy using ^{229}Th nuclei doped in VUV-transparent crystals. Here we extend the study of coherence and interference effects occurring in the interaction between coherent light and an ensemble of ^{229}Th nuclei towards two important directions. First, we consider a more realistic scenario than in Ref. [36] and take into account the effect of sample inhomogeneities that broaden the nuclear transition width. This broadening is incoherent and does not enhance the strength of the light-nucleus coupling; however, its effects need to be well understood and controlled for frequency standard applications. So far theoretical studies of the sources of width broadening in an ensemble of ^{229}Th nuclei consider the doping ^{229}Th ion occupying the same location in the crystal unit cell. The theoretical studies in Ref. [23] show that in a thorium-doped CaF_2 crystal, for instance, the thorium ion will most probably replace a Ca^{2+} ion in a Th^{4+} state. The broadenings experienced by the thorium nuclei due to electric and magnetic fields from the surrounding lattice are then assumed to be the same throughout the sample [23,36,37]. This is, however, difficult to achieve in practice not least due to impurities and color centers, which may occur even during the experiment as irradiation effects. Motivated by this, we investigate the effect of different ^{229}Th doping sites for the NFS response of the irradiated sample. This effect is shown to come into interplay with interference effects due to the hyperfine splitting of the ground and isomeric nuclear states leading to specific beating patterns in the scattered spectra. The effects of different nuclear sites for the fitting of iron ^{57}Fe Mössbauer spectra has been investigated in detail [38].

A second goal of this work is to extend the study of interference effects for the more realistic case of a multilevel quantum system to mimic the quadrupole hyperfine structure of ^{229}Th presented in Fig. 1. We investigate a number of possible two-, three- and four-level schemes involving quadrupole sublevels of the ground and isomeric nuclear states coupling to one or two coherent fields. For the case of three-level schemes we consider two different configurations: the so-called V configuration in which two excited hyperfine states couple to one ground state, and the Λ configuration where two ground hyperfine levels are coupled to one excited state. Both these level configurations have been extensively investigated in multilevel quantum optical studies of atoms and molecules. As driving fields we consider both pulsed and continuous-wave coherent VUV sources. We find specific configurations which offer clear signatures of the isomer excitation advantageous for the more precise experimental determination of the transition energy. Furthermore, it is shown that even population trapping into the isomeric state can be achieved in a two-field driven three-level V configuration. This paves the way for further nuclear quantum optics applications with ^{229}Th. The paper is organized as follows. In Sec. II we describe the model and discuss the basic properties of coherent forward scattering of VUV laser from an ideal system—an ensemble of two-level nuclei doped in a VUV-transparent crystal lattice environment. We then develop a general theoretical framework in terms of the Maxwell-Bloch formalism to study coherent forward scattering of VUV including decoherence, multiple resonances due to multilevel structure of nuclei, and inhomogeneity due to different doping sites. In Sec. III we then apply this framework to the study of NFS from an ensemble of two-level nuclei doped in a VUV-transparent crystal lattice environment affected by decoherence (for instance via spin-lattice relaxation) and doping inhomogeneity. In Sec. IV we consider an ensemble of multilevel nuclei doped in a crystal lattice environment in several different configurations driven by either one or two optical fields. In Sec. IV A we study NFS of a VUV pulse from a three-level scheme in which one hyperfine level of the isomeric state is coupled to two different hyperfine levels of the nuclear ground state by a probe and a control field. We consider both continuous-wave and pulsed fields as control field and discuss the corresponding quantum interference signatures in the NFS spectra. The effect of different ^{229}Th doping sites on the NFS signal in such a three-level setup is investigated. In Sec. IV C we study NFS of a VUV pulse from a three-level scheme in which two hyperfine levels of the isomeric state are coupled to a common hyperfine level of the nuclear ground state by a single optical field. We also investigate in this model the effect of coherence created between the hyperfine levels of the isomeric state on the population dynamics. In Sec. IV D we then study NFS of a VUV pulse driving a four-level configuration with two near-degenerate transitions. Finally we conclude in Sec. V with a summary of our findings.

II. MODEL AND THEORETICAL FRAMEWORK

We begin our investigation by studying NFS off an ensemble ^{229}Th nuclei doped in a crystal lattice environment. Nuclear spectroscopy using ^{229}Th nuclei doped in VUV-transparent crystals such as $LiCaAlF_6$ [37] or CaF_2 [23] offers the possibility to increase the nuclear excitation probability significantly due to the high doping density of up to 10^{18} Th/cm^3. Both $LiCaAlF_6$ and CaF_2 have large band gaps and present good transparency at the probable transition wavelength. Hence, interplay with electronic shells in processes such as the electronic bridge [39], internal conversion [40], or nuclear excitation via electron capture or transition [41] can be neglected. When confined to the Lamb-Mössbauer regime of recoilless nuclear transitions, the excitation of the isomeric transition will occur coherently in the forward direction. This then leads to speed-up of the initial nuclear decay depending primarily on the sample optical thickness. These effects are well known from NFS of synchrotron radiation [42,43] driving Mössbauer nuclear transitions in the x-ray regime, and have been addressed for the first time for the case of ^{229}Th in Ref. [36].

As nuclear level scheme we use the quadrupole structure of ^{229}Th with hyperfine level energies given by $E_m \simeq Q_{is(g)}(1-\gamma_\infty)\phi_{zz}[3m^2 - I_{is(g)}(I_{is(g)}+1)]/[4I_{is(g)}(2I_{is(g)}-1)]$. Here $Q_{is(g)} = 1.8$ eb (3.15 eb) is the quadrupole moment of the isomeric (ground) level, $\gamma_\infty = -(100\text{–}200)$ is the antishielding factor and $(1-\gamma_\infty)\phi_{zz} \sim -10^{18}$ V/cm^2 is the electric field gradient [23,25]. Figure 1 shows the energy scheme of ^{229}Th with the electric quadrupole splitting [23] of the ground and excited ^{229}Th nuclear states of spins $I_g = 5/2$ and $I_{is} = 3/2$, respectively. We use the recently proposed ^{229}Th:CaF$_2$ crystal [23] parameters for numerical evaluation of the NFS signal.

A radiation pulse denoted in the following as "probe" driving the relevant nuclear transition shines perpendicular to the nuclear sample, and the scattering response in the forward direction is recorded. Depending on the pulse polarization, different hyperfine transitions will be driven. This setup follows the typical NFS experiments extensively performed with ^{57}Fe [32,44].

A. Analytical framework: Two-level approximation

We consider first the simplest possible model for NFS study—two-level nuclei interacting with an incident VUV laser pulse. In case of ^{229}Th, such a two-level system can be formed by selectively driving a $m_e - m_g = 0, \pm 1$ magnetic dipole transition with a VUV pulse using a cooled sample where not all hyperfine ground states are populated. Here m_e and m_g denote the projections of the excited and ground state nuclear spins on the quantization axis, respectively. The VUV laser pulse may be generated via nonlinear sum-frequency mixing [45], or a harmonic of a VUV frequency comb [46,47] around the isomeric wavelength.

In NFS the resonant scattering off the nuclear ensemble occurs via an excitonic state—an excitation coherently spread out over a large number of nuclei. When the scattering is coherent, the nuclei return to their initial state, erasing in the process any information of the scattering path. This leads to cooperative emission with scattering only in the forward direction (except for the case of Bragg scattering [32,42,44]) and decay rates modified by the formation of sub- and super-radiant modes of emission. In combination with the narrow linewidth of nuclear transition, this cooperative feature of NFS has been exploited in studying cooperative Lamb shifts [48,49], single-photon entanglement generation in the x-ray regime [50,51], storage and modulation of single hard x-ray photons [27], and the coherent optical scheme of direct determination of the ^{229}Th isomeric transition [36]. The time evolution of the forward scattering response exhibits pronounced intensity modulations characteristic of the coherent resonant pulse propagation [43,52,53]. This modulation is known in nuclear condensed-matter physics under the name of dynamical beat and, for a single resonance (two-level approximation) and a short $\delta(t)$-like exciting pulse, has the form

$$E(t) \propto \xi e^{-\tau/2} J_1(\sqrt{4\xi\tau})/\sqrt{\xi\tau}, \tag{1}$$

where E is the transmitted pulse envelope, τ is a dimensionless time parameter $\tau = t/t_0$ with t_0 denoting the natural lifetime of the nuclear excited state, ξ is the optical thickness, and J_1 is the Bessel function of the first kind. The optical thickness is defined as $\xi = N\sigma L/4$ [32], where N is the number density of nuclei, σ is the nuclear resonance cross section, and L is the sample thickness. In the asymptotic limit, for early times of evolution $\tau \ll 1/(1+\xi)$, the response field has the form $E(t) \propto \xi \exp[-(1+\xi)\tau/2]$, showing the speed-up of the initial decay by ξ. At later times, the decay becomes subradiant, i.e., with a slower rate comparable to the incoherent natural decay rate due to destructive interference between radiation emitted by nuclei located at different depths in the sample.

In the case of ^{229}Th doped in VUV transparent crystals, both the conditions for recoilless, coherent excitation and decay and for broadband excitation are fulfilled for scattering in the forward direction. The incident VUV laser pulse duration is much shorter than the nuclear lifetime and provides broadband excitation. Since the crystal is expected to be transparent at the nuclear transition frequency [23], the main limiting factor for coherent pulse propagation, namely, electronic photoabsorption, is not present in this case. Thus we can expect pronounced intensity modulations characteristic of the coherent resonant pulse propagation given by the analytical expression (1) for the forward scattered field from an ensemble of two-level ^{229}Th nuclei.

B. General framework: Maxwell-Bloch formalism

Instead of using Eq. (1) to study the behavior of the scattered field intensity in the forward direction, we take an alternative approach and numerically evaluate the Maxwell-Bloch equations [5]. This allows us to include multiple transitions between hyperfine splitting levels in ^{229}Th (this will become important in later sections when we consider multiple levels) and consider decoherence processes such as inhomogeneous broadening occurring due to spin-spin relaxation. The interaction Hamiltonian for the system of multilevel nuclei in the dipole approximation and in a frame rotating with the frequency of the incident laser is given by

$$\mathcal{H} = \hbar \sum_j \Delta_j S_j^- S_j^+ - \sum_j \left(\frac{\Omega_j}{2} (\vec{\varepsilon}_{fj} \cdot \vec{\varepsilon}_{nj}) S_j^+ + \text{H.c.} \right), \tag{2}$$

where $\Delta = \omega_j - \omega_L$ is the so-called detuning with ω_j, ω_L being the jth nuclear transition and the driving laser frequency, respectively. Here Ω_j is the space- and time-dependent Rabi frequency of the driving field for the nuclear transition of interest labeled by j and $\vec{\varepsilon}_{fj}, \vec{\varepsilon}_{nj}$ are the polarizations of the incident light and of the transition, respectively. Furthermore, S_j^+ (S_j^-) are the nuclear raising (lowering) operators for the jth transition in analogy to the atomic raising (lowering) operators and satisfying the $SU(2)$ angular momentum algebra.

The interaction of the doped nuclei with their environment consisting of atoms, electrons and nuclei of other species in the VUV crystals leads to relaxation and decoherence in the system. The major mechanisms of relaxation and decoherence are the spontaneous decay—in the crystal assumed to occur only radiatively—and the spin relaxation of thorium nuclei due to interaction with the random magnetic field created by the surrounding fluorine spins in CaF_2 [23]. Mathematically the effect of population relaxation can be included in the formalism by the following Louvillian operators:

$$\mathcal{L}\rho^{(\alpha)} = -\sum_j \frac{\gamma_j}{2}\left(S_j^+ S_j^- \rho^{(\alpha)} + \rho^{(\alpha)} S_j^+ S_j^- - 2S_j^- \rho^{(\alpha)} S_j^+\right), \tag{3}$$

where γ_j is the population relaxation rate of the jth transition and $\rho^{(\alpha)}$ is the density operator for the nuclei of type α. The relaxation rate for a relevant nuclear hyperfine transition can be related to the total decay rate with the help of the corresponding Clebsch-Gordon coefficient [3]. In practice, due to more than one doping sites of the VUV crystal, the nuclear ensemble might consist of ^{229}Th nuclei with different hyperfine splittings, which can in principle be treated as different species of nuclei doped throughout the sample. The index α will be used to differentiate between the nuclei doped in different nuclear sites.

In order to obtain the NFS time spectra, we evaluate the net generated intensity $I(z,t) = |\Omega(z,t)|^2$ at the exit from the medium. The behavior of the output field $\Omega(z,t)$ is given by the Maxwell equations involving the induced nuclear currents which in turn are related to the coherence terms. The coherence in the system can be found by studying the dynamics of the density matrix $\rho^{(\alpha)}$. This thus leads to the coupled Maxwell-Bloch equations [5]

$$\partial_t \rho^{(\alpha)} = \frac{1}{i\hbar}[\mathcal{H}, \rho^{(\alpha)}] + \mathcal{L}\rho^{(\alpha)} + \mathcal{L}_d \rho^{(\alpha)}, \tag{4}$$

$$\partial_z \Omega_j + \frac{1}{c}\partial_t \Omega_j = i \sum_\alpha \sum_{lk} \eta_{lk}^{(\alpha)} a_{lk} \rho_{lk}^{(\alpha)}, \tag{5}$$

where a_{lk} is the Clebsh-Gordon coefficient, $\eta_{lk}^{\alpha} = \Gamma_0 \xi_{lk}^{(\alpha)}/2L$ for the transition between the states $l \to k$, $(l \neq k)$, and Γ_0 is the natural (radiative) decay rate for the nuclei. Note that the optical thickness ξ varies with the group index α and the transition, due to its dependence on the doping density and transition linewidth via the nuclear resonance cross section [54]. For typical ^{229}Th-doped VUV crystal parameters $\Gamma_0 \sim 0.07$ mHz, $\eta = 100$ Hz/cm, where $\xi = 10^6$ and $L = 1$ cm [1,23,36]. The term $\mathcal{L}_d\rho^{(\alpha)}$ in the above equations represents the decoherence of the relevant nuclear transitions for both few-level and multilevel nuclei.

III. COHERENCE EFFECTS IN NFS OFF AN ENSEMBLE OF TWO-LEVEL NUCLEI

In this section we investigate the properties of NFS of a VUV laser pulse off an ensemble of simple two-level ^{229}Th doped in a VUV-crystal lattice environment. This problem was discussed earlier in Sec. II in an analytical framework. Here, we use the general framework developed in the previous section to numerically simulate the additional effect of decoherence and different doping sites on the NFS for Th-doped VUV-transparent crystals.

We begin our investigation by assuming the exciting VUV pulse to be linearly polarized, and for now driving resonantly a single transition. Thus the hyperfine manifold of the ^{229}Th nucleus can be approximated by a two-level system satisfying the selection rule $m_e - m_g = 0$. For our model calculation we explicitly choose the levels to be $\{|3/2, -3/2\rangle = |1\rangle, |5/2, -3/2\rangle = |2\rangle\}$ as shown in Fig 2(a). Thus in the two-level situation the number of transitions

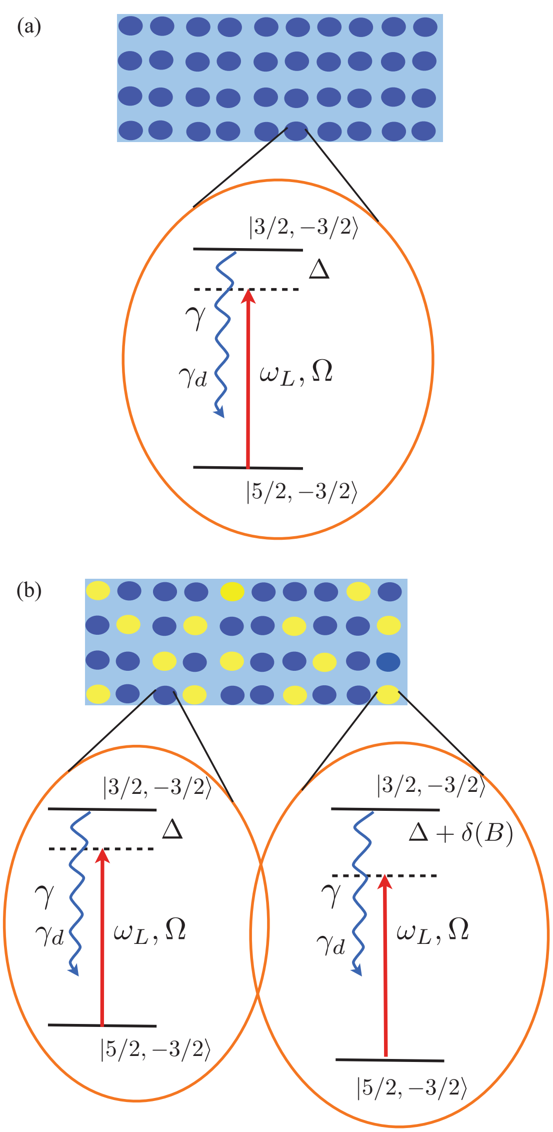

FIG. 2. (Color online) (a) Level scheme for VUV excitation of the doped ^{229}Th in the crystal lattice. All doping thorium nuclei share the same environment and lattice-generated fields. (b) Level schemes for two different doping sites. The darker (blue) thorium nuclei are influenced by a different environment than the lighter (yellow) ones. See text for further explanations.

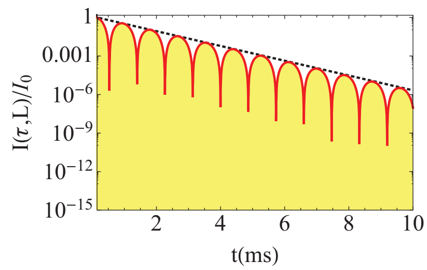

FIG. 3. (Color online) NFS time spectra scattered off an ensemble of two-level nuclei. The dotted (black) line shows the results for single-site doping while the solid (red) one with yellow shading is for two-site doping. Here $\gamma = 0.356\Gamma_0$, $\eta^{(1)} = \eta^{(2)} = \eta/2 \sim 91$ Hz/cm for $\xi = 10^6$ with the pulse and detuning parameters $\Omega_0 = 10^6\Gamma_0$, $t_0 = 0.1$ ms, $\tau = 0.01$ ms, and $\delta(B) = 10^{(8)}\Gamma_0$, respectively.

involved is only 1, and the nuclear raising and lowering operators are defined as $S^+ = |1\rangle\langle 2|$, $S^- = (S^+)^\dagger$. The corresponding field equation (5) is thus driven by a single coherence term $\rho_{12}^{(\alpha)}$ with the subscript j on Ω replaced by p denoting the probe field. Furthermore, the decoherence term $\mathcal{L}_d\rho^{(\alpha)}$ in Eq. (4) for the two-level configuration can be written as

$$\mathcal{L}_d\rho^{(\alpha)} = -\frac{\gamma_d}{2}(S^zS^z\rho^{(\alpha)} + \rho^{(\alpha)}S^zS^z - 2S^z\rho^{(\alpha)}S^z), \quad (6)$$

where γ_d is the decoherence rate of the transition and $S^z = 1/2(|1\rangle\langle 1| - |2\rangle\langle 2|)$ is the energy operator. For the present analysis we assume that all thorium nuclei occupy the same doping site in the VUV crystal, i.e., all dopants experience the same lattice fields and hence we can drop the index α. The coupled Maxwell-Bloch equations (4) and (5) are solved taking into account the initial condition that all the population is in the ground state [$\rho_{22}(0) = 1$]. The exciting VUV pulse is assumed to have a Gaussian shape defined by the initial and boundary conditions

$$\Omega_p(0,t) = \Omega_{p0}\exp\left[-\left(\frac{t-t_0}{\tau}\right)^2\right], \quad \Omega_p(z,0) = 0. \quad (7)$$

The NFS time spectrum after the passage of the excitation pulse is shown by the dotted line in Fig. 3 for a resonant probe field and with a decoherence (spin relaxation) rate of $\gamma_d = 2\pi \times 108$ Hz [23]. A Rabi frequency of $\Omega_0 = 10^6\Gamma_0$ is assumed for the numerical computation of the Maxwell-Bloch equations in the present case. Our result enforces the earlier found behavior of NFS spectra of ^{229}Th in such a setup [36]. The NFS time spectra are not sensitive to the laser detuning and have a behavior similar to that in Fig. 3 for a large range of detuning Δ (0–1 KHz). Furthermore, the slope of the time spectra essentially follows the decoherence rate $e^{-2\gamma_d t}$ of the two-level nuclear system.

A. Different doping sites

In the above case we have assumed that any energy shifts or broadening induced by the crystal lattice (such as hyperfine interactions) are the same for all thorium nuclei. However, in practice the perfectly doped crystal with all thorium nuclei in the same doping site is hard to achieve, since impurities and color centers are often also present. The energy splittings of the driven hyperfine transitions can therefore be different at different lattice sites.

We mimic this situation for a simple case by considering the VUV crystal with two groups of dopant nuclei with different splitting of the isomeric transition energy. In the Hamiltonian (2) the index j takes the values $j = 1, 2$ now, with $\Delta_1 = \Delta$ and $\Delta_2 = \Delta_1 + \delta(B)$ representing the second group of nuclei depicted by yellow circles in Fig. 2(b). Here $\delta(B)$ is an additional intrinsic magnetic-field-dependent detuning due to the different hyperfine splitting of the second group of nuclei. The incident field in this case interacts with both groups of dopant nuclei leading to simultaneous contribution of the nuclear coherences from each group in the generated signal. The field equation in the Maxwell-Bloch formalism changes accordingly to incorporate the contribution of coherences from both nuclear sites. In Eq. (5) the index $\alpha = 1, 2$ stands now for the two groups of doping thorium nuclei. The dynamics of the system follows from Eq. (4) with the modified Hamiltonian as discussed above and the corresponding population relaxation and decoherence given by Eqs. (3) and (6). For simplicity we have considered equal doping density of the groups such that $\eta^{(1)} = \eta^{(2)}$.

The NFS time spectrum for two different doping sites is shown in Fig. 3 by the solid line with yellow shading. We have assumed resonant driving of the transition for the first group of nuclei ($\Delta = 0$) and $\delta(B) = 10^8\Gamma_0$ corresponding to an intrinsic magnetic field of ∼100 gauss. The behavior of the time spectra is distinctly modified in the presence of such nonuniform doping. We find quantum beats in the NFS spectra of the order of $\delta(B)$ owing to internuclei quantum interference between the two groups with different hyperfine splittings. The beating pattern is influenced by the decoherence in the system and has an envelope governed by the decay rate $e^{-2\gamma_d t}$.

Unfortunately, in experiments such spectra cannot be differentiated from background coming from other unwanted electronic processes in the VUV crystal that can be active at nonresonant probe laser frequencies. The NFS signal lacks any distinctive signature of nuclear resonance, particularly for uniform doping of the sample, being insensitive to even large detunings. In the following sections we thus move on to some more complicated and realistic multilevel models of ^{229}Th in search for isomeric signatures provided by coherence and quantum interference features in the scattered light.

IV. COHERENCE EFFECTS IN NFS OFF AN ENSEMBLE OF MULTILEVEL NUCLEI

In this section we systematically study the effect of quantum coherence and interference on the NFS signal emitted from an ensemble of multilevel nuclei. In the first part of this section we consider a nuclear ensemble interacting with two fields which selectively drive two magnetic dipole transitions. The level configuration is such that in each nucleus there is one upper level connected to two lower levels by the two fields forming a Λ system. The Λ scheme is a typical set for interference effects and has been extensively studied in atomic quantum optics during the past decade. In the second part of the section we consider the inverse level configuration of the nuclear ensemble, i.e., a V configuration where a single field drives two transitions formed by two upper and one lower nuclear levels. A second additional field that couples the upper states is also considered in this case to create coherence among the latter. Finally in the last part we study a nuclear ensemble in which a single field drives two nearly degenerate transitions formed by four levels in a two-upper and two-lower states configuration.

A. Nuclear ensemble in a three-level Λ configuration

We consider an ensemble of nuclei occupying the same doping site in a VUV crystal interacting with two electromagnetic fields. One of the fields is a left-circularly polarized weak VUV pulse denoted in the following as "probe" driving the $m_e - m_g = -1$ magnetic dipole transition, while the other is a strong right circularly polarized continuous wave (cw) denoted as "control" driving the $m_e - m_g = 1$ transition. Due to the selected polarizations, the two fields couple two nuclear ground states to a common excited state forming a Λ-type scheme. Such a Λ configuration of the nuclear levels can be achieved in ^{229}Th by driving the transition $|5/2, \pm 1/2\rangle \rightarrow |3/2, \pm 3/2\rangle$ with the control laser and the $|5/2, \pm 5/2\rangle \rightarrow |3/2, \pm 3/2\rangle$ transition with the probe pulse as shown in Fig. 4(a). Note that recently such a three-level two-field scheme was proposed for the coherence-enhanced optical determination of the isomeric transition energy to a high precision [36].

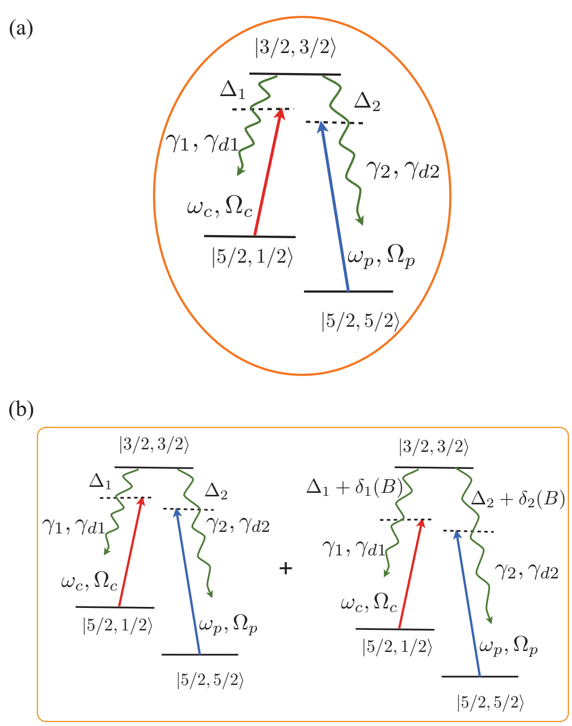

FIG. 4. (Color online) Level schemes of the doped ^{229}Th in the crystal lattice exposed to two VUV fields. (a) The doping occurs in one site only and thus all the thorium nuclei experience the same environment. (b) Two-site doping with different hyperfine splittings due to different magnetic environments in the crystal lattice. See text for further explanations.

For the three-level scheme, the interaction Hamiltonian is given by Eq. (2) with $j = 1, 2$ representing the transitions $|5/2, \pm 1/2\rangle \rightarrow |3/2, \pm 3/2\rangle$ and $|5/2, \pm 5/2\rangle \rightarrow |3/2, \pm 3/2\rangle$, respectively. The nuclear raising (lowering) operators are defined in a three-level basis $\{|3/2, \pm 3/2\rangle = |1\rangle, |5/2, \pm 1/2\rangle = |2\rangle, |5/2, \pm 5/2\rangle = |3\rangle\}$ as $S_1^+ = |1\rangle\langle 2|$, $S_2^+ = |1\rangle\langle 3|$, $S_k^- = (S_k^+)^\dagger$, $k = 1, 2$. In the following we consider the transitions between the states with positive angular momentum projection $|5/2, 1/2\rangle$, $|5/2, 5/2\rangle$, and $|3/2, 3/2\rangle$; similar results are valid when the fields couple the corresponding states with negative projections. There are two Rabi frequencies $\Omega_1 = \Omega_c$ and $\Omega_2 = \Omega_p$ in the Hamiltonian corresponding to the control and probe fields with the detunings $\Delta_1 = \omega_{12} - \omega_c$ and $\Delta_2 = \omega_{13} - \omega_p$, where ω_c, ω_p and ω_{12}, ω_{13} are the frequencies of the control, probe, and the relevant nuclear transitions, respectively. The population relaxations in the three-level system are given by the Louvillian operator in Eq. (3) with $j = 1, 2$ and γ_1 and γ_2 being the relaxation rates of the isomeric state to the two ground levels $|5/2, 1/2\rangle$ and $|5/2, 5/2\rangle$, respectively. All nuclei experience the same environment and hyperfine splitting such that we drop the index α on the density operator. The decoherence of the transitions are incorporated in the dynamical equations by means of the decoherence matrix,

$$\mathcal{L}_d \rho = - \begin{bmatrix} 0 & \gamma_{d1}\rho_{12} & \gamma_{d2}\rho_{13} \\ \gamma_{d1}\rho_{21} & 0 & 0 \\ \gamma_{d2}\rho_{31} & 0 & 0 \end{bmatrix}, \qquad (8)$$

where γ_{d1} and γ_{d2} are the decoherence rates of the transitions $|5/2, 5/2\rangle \rightarrow |3/2, 3/2\rangle$ and $|5/2, 1/2\rangle \rightarrow |3/2, 3/2\rangle$, respectively. We consider the system to be closed, thus enforcing no population relaxation of the ground states (no leakage of population from ground to other hyperfine states) in our model.

The Maxwell-Bloch equations for the three-level scheme are given by Eqs. (4) and (5) with $j = p$, $l = 1$, $k = 3$ in Eq. (5) and without the summation over index α. The coherence ρ_{13}, i.e., the source term in the field equation, is evaluated from the Bloch equation (4). The second term of the Maxwell-Bloch equations only involves the probe field as the control field is assumed to be a continuous wave. Time spectra of the NFS are numerically evaluated as the scattered intensity of the probe field from the Maxwell-Bloch equations.

For numerical computation we have considered the initial condition $\rho_{33}(0) = 1$ for the Bloch equations. The initial and boundary conditions on the probe field are given by Eq. (7) with $\Omega_{p0} = 10^6\Gamma_0$. The Rabi frequency of the control field is assumed to be $10^2\Omega_{p0}$ which is of the order of MHz. Furthermore, as the quadrupole splitting of the thorium ground state can be determined experimentally [23], following [36] we set the detunings of the control and probe fields to be identical, i.e., $\Delta_1 = \Delta_2 = \Delta$. The time spectrum of the field intensity scattered in the forward direction is shown in Fig. 5 by the dashed black curve with yellow shading for decoherence rates $\gamma_{d1} = 2\pi \times 158$ Hz, $\gamma_{d2} = 2\pi \times 251$ Hz and detuning $\Delta = 10^5\Gamma_0$. The spectrum as seen from the figure is quite

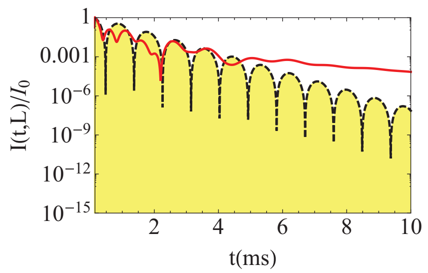

FIG. 5. (Color online) The time domain spectrum of NFS for a Λ three-level configuration with two-fields setup. The black dotted (solid red) curve with yellow shaded region represents the scattering signal for single (two-site) doping. Here we have considered equal doping density for the two nuclear sites such that $\eta_{13}^{(1)} = \eta_{13}^{(2)} = \eta_{13}/2 \simeq 227$ Hz/cm for $\xi \simeq 10^6$. The additional detuning introduced by the two different doping sites is $\delta_i(B) = 10^8\Gamma_0$. The spontaneous decay rates of the transitions are respectively $\gamma_1 = 0.088\Gamma_0$ and $\gamma_2 = 0.889\Gamma_0$. The control and probe fields are equally detuned from the level $|3/2, 3/2\rangle$ by $\Delta = 10^5\Gamma_0$. The control field is assumed to have a Rabi frequency of $10^8\Gamma_0$.

different to that of the two-level case with uniform doping. Here we observe definite signatures of nuclear excitation in the form of quantum beats in the NFS signal [32,36]. Furthermore, the beats are influenced by decoherence of the probe transition and have an envelope governed by the rate $e^{-2\gamma_{d2}t}$.

The existence of the quantum beats in such a three-level configuration can be explained in the dressed-state picture [55]. The strong control field dresses the transition $|5/2, 1/2\rangle \rightarrow |3/2, 3/2\rangle$ to form two new dressed states $|\Psi_+\rangle$ and $|\Psi_-\rangle$ which are linear combinations of the states $|3/2, 3/2\rangle$ and $|5/2, 5/2\rangle$ such that

$$\begin{aligned} |\Psi_+\rangle &= \sin\theta|5/2, 1/2\rangle + \cos\theta|3/2, 3/2\rangle, \\ |\Psi_-\rangle &= \cos\theta|5/2, 1/2\rangle - \sin\theta|3/2, 3/2\rangle, \end{aligned} \tag{9}$$

where $\tan(2\theta) = \Omega_c/\Delta$. The incoming probe excitation then couples these two dressed states to the $|5/2, 1/2\rangle$ level. Thus the nuclear resonance driven by the probe field is split into a doublet [56] via the Autler-Townes effect [57], forming two transition pathways for emission. The quantum interference for emission along these two transitions creates the beating pattern with the dressed frequency $\tilde{\Omega}$, where $\tilde{\Omega} = \sqrt{\Delta^2 + \Omega_c^2}$. As in the present case $\Delta \ll \Omega_c$, the dressed frequency is approximately the same as the Rabi frequency of the control field. Note that the beating pattern found in this case is similar to the two-level situation with two-site doping. This is due to the fact that in both cases the NFS involves two transition pathways with frequency difference of $10^8\Gamma_0$. The physical origin of the quantum beats is, however, different. While the beats arise due to intranuclei quantum interference in the three-level case with uniform doping, for the two-level case with two doping sites they come about as a result of internuclei quantum interference.

So far we have assumed only one doping site for the three-level system. For a two-doping site situation the Hamiltonian description of the Λ configuration now comprises two Hamiltonians of the form (2) for group 1 and 2 of doping nuclei, respectively. The detuning Δ_j in the Hamiltonian for the second group, however, has now additional terms $\Delta_1 \rightarrow \Delta_1 + \delta_1(B)$ and $\Delta_2 \rightarrow \Delta_2 + \delta_2(B)$. Here $\delta(B)$ is an additional intrinsic magnetic field B dependent detuning due to the different hyperfine splitting of the second group of nuclei. The probe VUV pulse will now simultaneously interrogate both doping groups, with the field equation having nuclear coherence contributions from both doping sites 1 and 2. The index α on the density operator and η now takes the values $\alpha = 1, 2$ representing the nuclei in the two doping sites. The field equation for propagation in this case is given by Eq. (5) with the summation running over different values of α,

$$\partial_z\Omega_p + \frac{1}{c}\partial_t\Omega_p = ia_{13}\left(\eta_{13}^{(1)}\rho_{13}^{(1)} + \eta_{13}^{(2)}\rho_{13}^{(2)}\right). \tag{10}$$

The dynamics of the two groups of nuclei follows from Eq. (4) with $\alpha = 1, 2$ and the modified Hamiltonian as discussed above. The corresponding population relaxation and decoherence are given by Eqs. (3) and (8) for each α. We assume for computational purposes $\delta_1(B) = \delta_2(B) = \delta = 10^8\Gamma_0$ which corresponds to a magnetic field of $B = 100$ gauss. Furthermore, we take equal doping density for both nuclear sites such that $\eta_{13}^{(1)} = \eta_{13}^{(2)}$.

The red solid curve of Fig. 5 shows the NFS time spectrum in this case for equal doping density of the two nuclear sites. The spectral response is found to be distinctly different from the homogeneous case due to an interplay of two scenarios of quantum interferences. We label these as intra- and internuclei interference, the former due to the Autler-Townes splitting of the resonances with formation of dressed states (9) for each group of the nuclei, and the latter due to the two different sets of nuclei with different hyperfine splittings. As $\delta_i(B) \sim \Omega_c$ the intra-nuclei quantum interference in the two groups of nuclei with and without $\delta_i(B)$ is of the order of $\sqrt{2}\Omega_c$ and Ω_c respectively. In Fig. 5 we find the initial beating pattern as a result of interference between two groups of nuclei with different frequencies which, however, is smeared out gradually with time. Furthermore, contrary to the uniform doping case, at longer times the behavior of the NFS time spectrum is no longer governed by the decoherence rate of the probe transition. This feature can be attributed to loss of coherence among scattered field amplitudes from the two groups of nuclei with different detunings. The shallower slope in this case thus suggests that the system encounters an additional inhomogeneous broadening owing to the two different doping sites. Note that such distinct behavior of NFS with two-site doping arise only when $\delta_i(B) \geqslant \Omega_c$. In the other limit, the Autler-Townes splitting dominates and the nuclei in both sites would experience a beating $\sim\Omega_c$ and would become indiscernible, thereby resulting in a NFS time spectrum similar to that of a uniformly doped sample.

B. Pulsed control field

In the above discussion we have assumed that the control field is a continuous wave. However, a cw laser source in the VUV region is currently available only within limitations. The

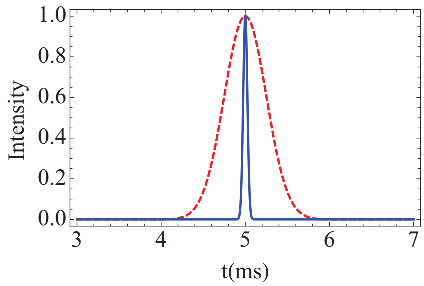

FIG. 6. (Color online) Time domain pulse shape of the control and probe fields shown by the dashed (red) and solid (blue) line. The control pulse has 10 times the width of the probe pulse with $\Omega_{c0} = 10^8\Gamma_0$ and $t_{c0} = 5$ ms, $\tau_c = 0.5$ ms, while the probe parameters are $\Omega_{p0} = 10^6\Gamma_0$ and $t_{p0} = 5$ ms, $\tau_p = 0.05$ ms, respectively.

$KBe_2BO_3F_2$ crystals [58] have been successful in generating narrow-band VUV radiation via harmonic generation owing to their wide transparency and large birefringence necessary for phase-matched frequency conversion processes in this frequency region [59,60]. A quasi-cw coupling VUV laser at around 160 nm wavelength could also be generated by the sum frequency mixing in metal vapors or driving a $KBe_2BO_3F_2$ crystal with a Ti:sapphire laser [59,61]. To circumvent these limitations we propose to use a VUV pulse of width much broader than the VUV probe pulse, allowing complete overlap of the two in the time domain as shown in Fig. 6.

Both control and probe Rabi frequencies in the Bloch equations (4) are in this case space and time dependent. Hence, the field equations for propagation (5) now have to be solved for both probe and control with additional initial and boundary conditions for the control field given by

$$\Omega_c(0,t) = \Omega_{c0} \exp\left[-\left(\frac{t-t_{c0}}{\tau_c}\right)^2\right], \quad \Omega_c(z,0) = 0. \quad (11)$$

The NFS signal is measured solely from the scattering of the probe pulse with the control pulse influencing the dynamics during its presence by formation of a time-dependent dressed state. In principle, by varying the overlap time of the probe and control pulses one can achieve stimulated Raman adiabatic passage (STIRAP) in this configuration. This has already been proposed for such configuration of nuclear levels involving keV and MeV transition energies in Refs. [4,29].

In Fig. 7 the black dotted curve shows the time spectrum of NFS from ^{229}Th doped VUV crystal for one doping site with both control and probe as pulsed fields. During the time when the control field is present the behavior of the NFS spectra is quite similar to that seen in Fig. 5, and we see the formation of a quantum beat. However, once the control and probe no longer overlap at $t \sim 6$ ms, the spectra become similar to those of two-level nuclei without any sensitivity to the probe detuning as discussed earlier. This time-dependent behavior of the beating is related to the time dependence of the dressed frequency $\tilde{\Omega}(t)$ [11,62] and of the dressed states (9). The time-dependent splitting of the resonances creates two transitions for the probe to interact with for the duration of the control pulse and determines the emission characteristics.

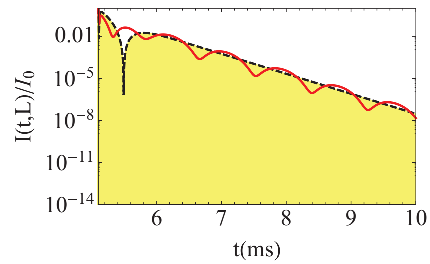

FIG. 7. (Color online) The time-domain spectrum of NFS for three-level configuration with a two-pulsed-field setup. The black dotted with yellow shading (red solid) curve is for a single-doping (two-doping) site case. Due to doping at a different site an additional shift of $\delta_2(B) = 10^8\Gamma_0$ of the energy level is induced in the second group of nuclei. Here we have considered equal doping density for the two groups such that $\eta_{13}^{(1)} = \eta_{13}^{(2)} = \eta_{13}/2 \simeq 227$ Hz/cm and $\eta_{12}^{(1)} = \eta_{12}^{(2)} = \eta_{12}/2 \simeq 22.7$ Hz/cm for $\xi \simeq 10^6$. The spontaneous emission rates are the same as those of Fig. 5. The control and probe fields are equally detuned from the level $|3/2, 3/2\rangle$ by $\Delta = 10^5\Gamma_0$.

As for the long-time behavior of the NFS spectra, it is found to be similar to the two-level case, with the response being dominated by the decoherence rate of the probe transition.

For the case of two doping sites in the VUV crystal, the space- and time-dependent propagation of the control field now has contributions from coherences of both groups. Thus the field equations in this case become

$$\begin{aligned} \partial_z\Omega_p + \frac{1}{c}\partial_t\Omega_p &= i a_{13}\left(\eta_{13}^{(1)}\rho_{13}^{(1)} + \eta_{13}^{(2)}\rho_{13}^{(2)}\right), \\ \partial_z\Omega_c + \frac{1}{c}\partial_t\Omega_c &= i a_{12}\left(\eta_{12}^{(1)}\rho_{12}^{(1)} + \eta_{12}^{(2)}\rho_{12}^{(2)}\right), \end{aligned} \quad (12)$$

with the Bloch equations given by (5), where the Hamiltonian now has an additional intrinsic magnetic-field-dependent detuning $\delta_i(B)$ $(i = 1, 2)$ for the second group of nuclei as was discussed at length for the case of a cw control field. For simulation we consider equal doping density for the two groups such that $\eta_{12}^{(1)} = \eta_{12}^{(2)}$ and $\eta_{13}^{(1)} = \eta_{13}^{(2)}$.

The NFS time spectrum is obtained from the field equation for the probe as shown by the solid (red) curve in Fig. 7. For a short time when the probe and control pulses overlap, we find the behavior similar to that of Fig. 5 governed by the interplay of two quantum interferences. The intranuclei interference arises from the two transitions created by time-dependent dressed states, while the internuclei interference comes into play due to different hyperfine splitting in two groups of ^{229}Th nuclei occupying the two different nuclear sites. However, once the control field and the probe cease to overlap, the dressed states and Autler-Townes doublet vanish. Thus, there is no further intranuclei interference and the NFS probe response bears the signature of only internuclei interference among the two groups of nuclei with different hyperfine splittings owing to different doping sites. Note that this behavior is similar to the two-level case, as in absence of the control field the probe simply interacts with a single transition in the nuclei. Furthermore, the envelope of the beating pattern is found to

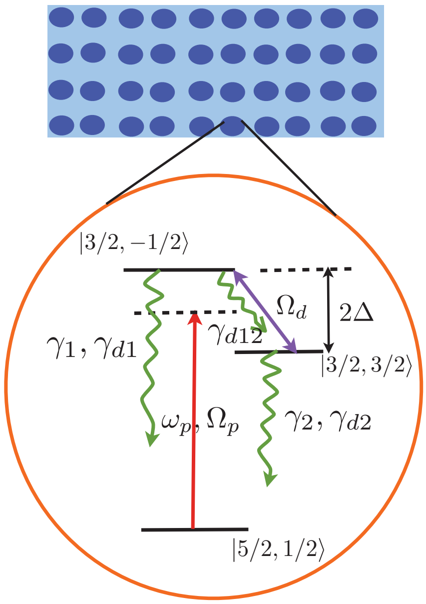

FIG. 8. (Color online) VUV excitation of the doping thorium nuclei in a three level V-configuration. The pulse with frequency ω_p is equally detuned from the upper doublet by Δ. The time-dependent driving pulse $\Omega_d(t)$ creates a time-dependent coherent superposition of the upper levels. Population trapping in the excited doublet occurs as long as drive and probe pulse overlap. See text for further explanations.

follow the decoherence rate of the probe transition in analogy to the simple two-level case.

C. Nuclear ensemble in a three-level *V* configuration

We next consider an ensemble of doping nuclei in the VUV-transparent crystal driven by a strong VUV probe pulse that couples two nearly degenerate upper levels to a common ground level forming a V configuration as shown in Fig. 8. Such a V-level scheme has been extensively investigated in atomic quantum optics. For instance, it was shown that, under the restrictive condition of nonorthogonality of the dipole transitions, decay-induced coherence among the upper levels is generated in such a scheme [63,64]. This coherence may lead to fascinating phenomena such as lasing without inversion [12], breaking of detailed balance [65] and manipulation of resonance profiles [66]. However, in our system the magnetic dipole transitions from the two upper to a common lower nuclear state are left and right circularly polarized and therefore orthogonal. To drive both transitions with a common field it is thus important to select the suitable polarization of the VUV pulse, which in this case is chosen to be along the $\hat{x}$ direction. Here we are interested in achieving population trapping among the upper levels by creating initial coherence among them via an additional VUV pulse as depicted in Fig. 8. In the following we denote this additional field as the driving field. The interaction Hamiltonian in the dipole approximation and in a frame rotating with the frequency ω_p of the probe for the V scheme has a form similar to Eq. (2) with $j = 1, 2$ and the interaction part modified to

$$\begin{aligned}\hbar \sum_j \left(\frac{\Omega_j}{2} (\vec{\varepsilon}_{fj} \cdot \vec{\varepsilon}_{nj}) S_j^+ + \text{H.c.} \right) \\ \rightarrow \hbar \frac{\Omega_p[z,t]}{2} [(\hat{x} \cdot \vec{\sigma}_-) S_1^+ + (\hat{x} \cdot \vec{\sigma}_+) S_2^+] \\ - \hbar \frac{\Omega_d}{2} [S_1^+ S_2^-] + \text{H.c.},\end{aligned} \tag{13}$$

where $\vec{\sigma}_\pm = (\hat{x} \pm i\hat{y})$, and Ω_p and Ω_d are the Rabi frequencies of the probe and driving field, respectively. The detunings in the Hamiltonian (2) are now $\Delta_1 = \omega_{13} - \omega_p$ and $\Delta_2 = \omega_p - \omega_{23}$, and the nuclear raising (lowering) operators are defined in the three-level basis $\{|3/2,-1/2\rangle = |1\rangle, |3/2,3/2\rangle = |2\rangle, |5/2,1/2\rangle = |3\rangle\}$ as $S_1^+ = |1\rangle\langle 3|$, $S_2^+ = |2\rangle\langle 3|$, $S_k^- = (S_k^+)^\dagger$, with $k = 1, 2$. The population relaxation in the V-level configuration is given by the Louvillian operator (3) with γ_1 and γ_2 being the population relaxation rates of the nuclear levels $|3/2,-1/2\rangle$ and $|3/2,3/2\rangle$ to the common ground levels $|5/2,1/2\rangle$, respectively. The decoherence of the relevant transitions is incorporated into the dynamics phenomenologically by means of the decoherence matrix

$$\mathcal{L}_d \rho = - \begin{bmatrix} 0 & \gamma_{d12}\rho_{12} & \gamma_{d1}\rho_{13} \\ \gamma_{d12}\rho_{21} & 0 & \gamma_{d2}\rho_{23} \\ \gamma_{d1}\rho_{31} & \gamma_{d2}\rho_{32} & 0 \end{bmatrix}, \tag{14}$$

where γ_{d12}, γ_{d1}, and γ_{d2} are the decoherence rates of the transitions $|1\rangle \rightarrow |2\rangle$, $|1\rangle \rightarrow |3\rangle$, and $|2\rangle \rightarrow |3\rangle$, respectively.

To obtain the NFS time spectra from the nuclear ensemble in such a V-level scheme we numerically compute the output field from the Maxwell-Bloch equations (5) and (6) without summation over the index α (we consider a single-doping-site scenario for this scheme) and with $j = p,\ l = 1, 2,\ k = 3$. The field propagation equation becomes

$$\partial_z \Omega_p + \frac{1}{c} \partial_t \Omega_p = i(\eta_{13} a_{13} \rho_{13} + \eta_{23} a_{23} \rho_{23}), \tag{15}$$

with contributions from coherences along both the transitions. The NFS time spectra generated by numerical computation of (15) and the Bloch equations are shown in Fig. 9. Here we have assumed the probe field, given by Eq. (7), to be positively and

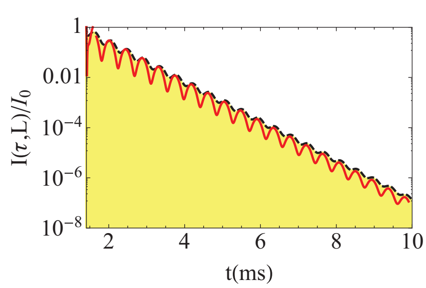

FIG. 9. (Color online) The time domain spectrum of NFS for three-level V configuration in a two-field setup. The black dotted (red solid) curve is in the absence (presence) of the external field coupling between the upper doublet. The parameters used for computation are $\gamma_1 = 0.267\Gamma_0$, $\gamma_2 = 0.0889\Gamma_0$, $\eta_{13} \simeq 22.7$ Hz/cm, $\eta_{23} \simeq 68$ Hz/cm for $\xi \simeq 10^6$, $\Omega_{d0} = 10^8\Gamma_0$, $t_{d0} = 1$ ms, $\tau_d = 0.1$ ms, $\Omega_{p0} = 10^9\Gamma_0$, $t_{p0} = 1.1$ ms, and $\tau_p = 0.1$ ms.

negatively detuned by $\Delta = 10^8\Gamma_0$ from the levels $|3/2, 3/2\rangle$ and $|3/2, -1/2\rangle$ respectively, and that all the population is initially in the ground state $\rho_{33}(0) = 1$. The decoherence rates are taken as $\gamma_{d12} = 2\pi \times 45$ Hz, $\gamma_{d1} = 2\pi \times 158$ Hz, and $\gamma_{d2} = 2\pi \times 142$ Hz in accordance with the estimates for ^{229}Th in CaF_2 [23]. For numerical purposes we have assumed that the driving field which couples the upper levels has a Gaussian shape,

$$\Omega_d(t) = \Omega_{d0} \exp\left[-\left(\frac{t - t_{d0}}{\tau_d}\right)^2\right]. \tag{16}$$

The dotted black curve in Fig. 9 shows the behavior of the NFS time spectrum in the absence of any coupling of the upper levels and after passage of the excitation pulse. We find quantum beat features owing to intranuclei quantum interference among the two transitions of the V configuration. The beats are of the order of 2Δ with an envelope governed by the highest decoherence rate in the system. The red solid curve in Fig. 9 depicts the behavior of NFS time spectra, when the upper levels are coupled by the driving field Ω_d which overlaps with the probe for a short period of time ($\sim$0.1 ms). The quantum beat pattern that we find in this case is similar to that found in absence of the driving field, however now with enhanced amplitudes. Thus the presence of coupling among the upper doublet does not show any significant influence on the probe NFS spectrum. This can be understood as follows. The probe field overlaps with the driving field for a very short time during its propagation through the medium, and thus any influence on the NFS spectrum will be transient and may be visible only at small scattering times. Furthermore, the decoherence of ρ_{12} spoils the coherence effects within ms of the its creation thereby erasing any signature of possible interplay of the two fields in the NFS spectra. Finally, considering the drive field to be strong enough to form a dressed state of the upper doublet like that discussed earlier for the Λ configuration, for parameters used in the figure the dressed frequency would be on the same order as the probe detuning Δ. Hence, no additional beating induced during the pulse overlap would be observed.

Although we do not see any dominant signature of the coherence among the upper doublet in the NFS spectra, a study of the population dynamics of the upper states shows that population trapping is achieved. In Fig. 10 we plot the populations of the upper states ρ_{11} and ρ_{22} in the presence (b),(d) and absence (a) of the driving field. Without driving field among the states $|1\rangle$ and $|2\rangle$ we find in Fig. 10(a) that for a strong excitation probe ($\Omega_{p0} = 10^9\Gamma_0 = 0.1$ MHz) the populations undergo Rabi oscillations between the states $|1\rangle \to |3\rangle$ and $|2\rangle \to |3\rangle$ during the pulse duration. The population dynamics is seen to be exactly the same for the two upper states. When the excitation pulse is gone, the ground state $|3\rangle$ remains mainly populated with about 5% of population in the upper states. The flat tail arises because these remaining population decays with the isomeric half-life that is much longer than our (ms) timescale. However, this behavior changes significantly in presence of the driving field coupling the states $|1\rangle$ and $|2\rangle$, and the population dynamics becomes dependent on the relative strength of the drive and the probe.

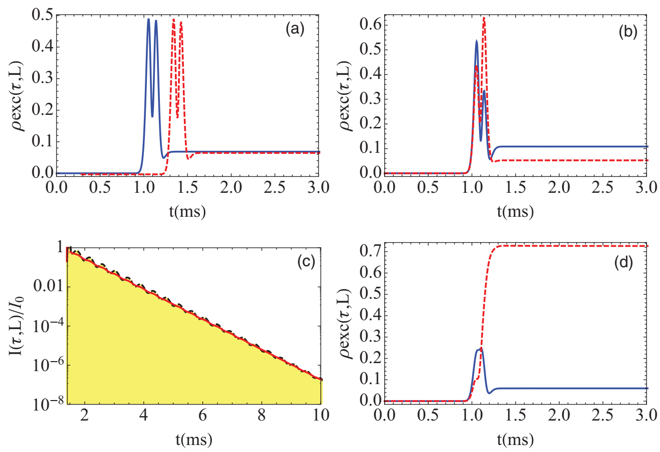

FIG. 10. (Color online) Population dynamics of the upper state doublets in V-configuration in (a) the absence and (b),(d) the presence of coherent coupling among the upper states. The solid (blue) and dashed (red) curves illustrate ρ_{11} and ρ_{22}. The amplitude of the driving field is different in (b) and (d), being respectively $\Omega_d = 10^8\Gamma_0$ and $\Omega_d = 10^9\Gamma_0$. All other parameters are the same as in Fig. 9. In (a) the dashed (red) line is shifted along the time axis by 0.5 ms for better visibility. (c) shows the NFS spectra corresponding to the population dynamics in (d).

For a weaker driving field compared to the probe $\Omega_d = 0.1\Omega_{p0}$, we see in Fig. 10(b) that the population dynamics of the upper doublet is no longer symmetric for the probe pulse duration. The drive creates a coupling between the states $|1\rangle$ and $|2\rangle$ via the coherence ρ_{12} which leads to population exchange among the states once any one of them is populated. The time-dependent dynamics then shows pronounced asymmetry in the Rabi oscillations of the two states as can be seen in the figure. The generated coherence is strongly influenced by the decoherence of the $|1\rangle \leftrightarrow |2\rangle$ transition and depends on the Rabi frequency of the driving field. In the present case it is weak due to a weaker Rabi coupling and is short lived due to the decoherence effect. Thus at later times, when the probe and drive cease to overlap, we find only 10% and 5% of the initial population still remaining in the upper states $|1\rangle$ and $|2\rangle$, respectively. The remaining population then decays with the isomeric half-life ($\sim$ hours) that is much longer than our (ms) timescale. Thus effectively we have moderately enhanced the trapped population in $|1\rangle$ due to the initial coherence among the doublet upper states.

The behavior of the upper states populations dramatically changes, however, when the driving field has a strength of the order of the probe field. The created coherence is stronger and leads to strong coupling between the upper doublet states even though it is short lived due to decoherence. Figures 10(c) and 10(d) illustrate the NFS spectra and the population dynamics, respectively. From Fig. 10(d) we see that the population of ρ_{11} increases gradually during the overlap of the probe and drive fields but then starts decreasing as the fields separate. Here ρ_{11} essentially shows a Lorentzian absorption peak in the presence of both the fields with small amount of population left in their absence. The population that goes in ρ_{11} due to strong coupling to $|2\rangle$ gets quickly distributed between the two upper states.

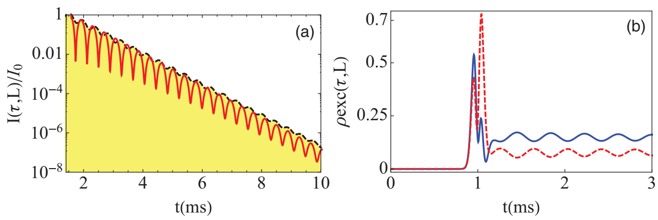

FIG. 11. (Color online) (a) NFS time spectra in the absence (dashed black line with shading) and presence (solid red line) of an external DC field coupling of the upper level doublet. (b) The solid (blue) and dashed (red) curves illustrate ρ_{11} and ρ_{22} when the upper states are coupled by a DC field with Rabi frequency $\Omega_d = 10^8\Gamma_0$. All other parameters are considered to be same as for Fig. 9.

In addition, state $|2\rangle$ becomes more and more populated as ρ_{11} decreases due to decoherence of ρ_{12}. As such, while ρ_{22} increases gradually when drive and probe overlap and attains a value similar to ρ_{11} when the fields gradually separate, it does not decrease and rather accumulates further population which eventually gets trapped due to long isomeric lifetime. We see from Fig. 10(d) that almost 70% of the total population gets trapped in state $|2\rangle$. The obtained trapping persists for a long time as seen by the flat tail of the population since $|2\rangle$ decays with isomeric half-life which is much longer than the (ms) timescale considered for our NFS calculations.

In Fig. 11 we plot the NFS time spectrum and the population dynamics for the V configuration with a DC drive field coupling the upper-level doublets. The behavior of the NFS spectra as seen from the red solid curve in Fig. 11(a) is similar to that of Fig. 9 for a pulsed driving field. In the DC field case the only difference is a larger beating amplitude. The similarity arises due to the fact that the dressing of the upper doublets with the DC field gives a dressed frequency of the same order of Δ for the considered parameters and thus no additional features appear in the NFS spectra. If, however, the Rabi frequency of the DC field were such that the dressed frequency were $\gg\Delta$, then the beating frequency would be given by the dressed frequency in the NFS spectra. The population dynamics of the upper state doublet in the presence of the DC field coupling is shown in Fig. 11(b). We find the behavior of the population to be similar to the case when the doublet was coupled by a pulse driving field for the probe duration; see Fig. 10(b). However, for longer times we find population oscillation of the states $|1\rangle$ and $|2\rangle$ otherwise absent in the pulsed field coupling case. Furthermore, we find almost 15% and 10% of initial population trapped in the $|1\rangle$ and $|2\rangle$ states.

In practice, one can achieve population trapping in the overlap region of the two laser focal spots. Considering experimentally realizable spot sizes for VUV lasers [37], we expect about 10^{11} nuclei to be addressed for a 0.1 cm ensemble depth. Thus almost 10^{10} nuclei can be trapped in state $|2\rangle$ and decay with the natural lifetime of the isomeric state despite the NFS setup. This in principle can be harnessed towards creating controlled subradiance in such nuclear isomers. Note that a similar subradiance phenomenon has been recently shown in a dilute cloud of cold atoms [67]. Thus, further studies in this direction contribute to the new field of collectivity-induced quantum optical phenomena in nuclear isomers.

D. Nuclear ensemble in a four-level configuration

In the case of ^{229}Th, the nuclear level structure will have more than two or three specific levels owing to the hyperfine interactions with the possibility of multiple transitions sharing the same polarization. Additionally, the spacing between hyperfine levels for a particular angular momentum I can be such that they cannot be resolved with the current bandwidth of lasers. All these conditions warrant the study of NFS from nuclear ensembles with multiple transitions which are either degenerate or near degenerate. Such studies have been already done extensively in ^{57}Fe—which is also a favorable test bed of several other studies related to NFS in nuclei. Here, we investigate the NFS time spectra of ^{229}Th in a similar spirit with the objective to find signatures of coherence and quantum interference present due to multiple transition pathways. We consider in the following a basic model of four-level nuclei with two upper and two lower nuclear levels as shown in Fig. 12(a). The nuclear levels are chosen such that given the selection rules and polarization of the incident VUV pulse only two parallel and near degenerate magnetic dipole transitions $|1\rangle \to |3\rangle$ and $|2\rangle \to |4\rangle$ are driven. For ^{229}Th such a four-level model can be formed by the states $\{|3/2, 3/2\rangle, |3/2, 1/2\rangle, |5/2, 5/2\rangle, |5/2, 3/2\rangle\} = \{1, 2, 3, 4\}$ driven by a left circularly polarized VUV laser pulse. Since for now we consider only one doping site in the VUV crystal we drop the index α on the density operator in the further discussion.

The interaction Hamiltonian for our four-level model in the dipole approximation and in a frame rotating with the probe laser frequency ω_p is given by Eq. (2) with $j = 1, 2$ for the two possible transitions. The nuclear raising (lowering) operators are now defined in a four-level basis as $S_1^+ = |1\rangle\langle 3|$, $S_2^+ = |2\rangle\langle 4|$, $S_k^- = (S_k^+)^\dagger$, $(k = 1, 2)$. The laser detunings in the Hamiltonian are $\Delta_1 = \omega_{13} - \omega_p$, $\Delta_2 = \omega_{24} - \omega_p$, respectively, and the Rabi frequency is assumed to be the same for both transitions, $\Omega_1 = \Omega_2 = \Omega_p$. The population relaxation of the hyperfine levels of the isomeric state is included in the dynamics by the Louivillian operator (3) with $j = 1, 2$, where now γ_1 and γ_2 are the decay rates of the levels $|1\rangle$ and $|2\rangle$ to $|3\rangle$ and $|4\rangle$, respectively. The effect of environmental decoherence is incorporated in the dynamics of the model phenomenologically via the decoherence matrix

$$\mathcal{L}_d\rho = -\begin{bmatrix} 0 & 0 & \gamma_{d1}\rho_{13} & 0 \\ 0 & 0 & 0 & \gamma_{d2}\rho_{24} \\ \gamma_{d1}\rho_{31} & 0 & 0 & 0 \\ \gamma_{d2}\rho_{42} & 0 & 0 & 0 \end{bmatrix}, \qquad (17)$$

where γ_{d1} and γ_{d2} are the decoherence rates of the transitions $|1\rangle \to |3\rangle$ and $|2\rangle \to |4\rangle$, respectively.

To obtain the time spectra of the NFS signal from the nuclear ensemble in such a four-level scheme we numerically evaluate the output field from the Maxwell-Bloch equations (4) and (5) where now the field equation (5) contains contributions from coherences along both transitions,

$$\partial_z\Omega_1 + \frac{1}{c}\partial_t\Omega_1 = i(a_{13}\eta_{13}\rho_{13} + a_{24}\eta_{24}\rho_{24}). \qquad (18)$$

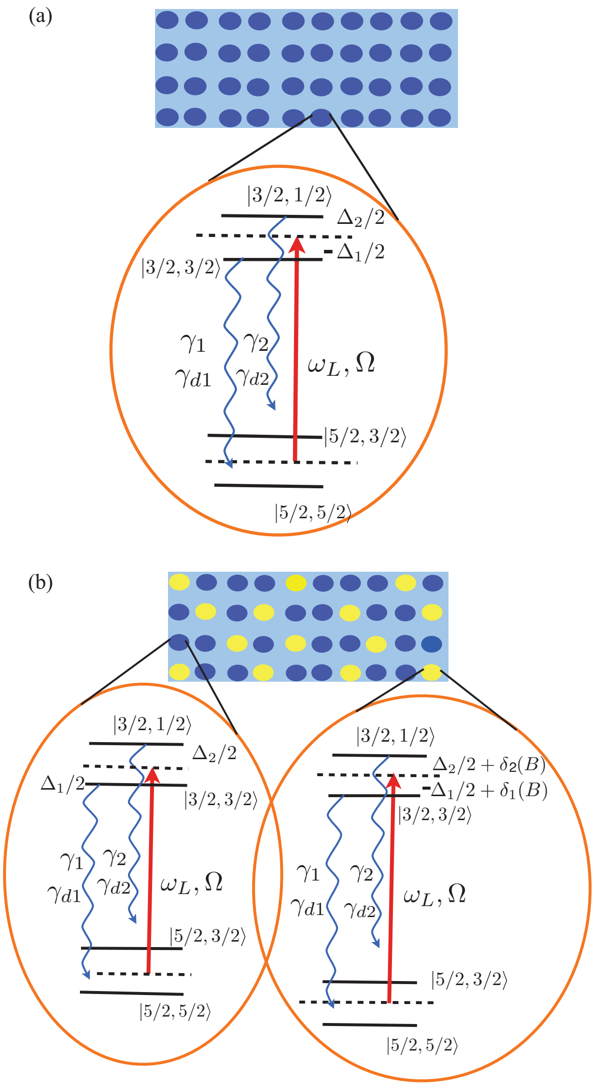

FIG. 12. (Color online) (a) VUV excitation of the doped ^{229}Th in the crystal lattice in the case of a single doping site. The laser with frequency ω_c is tuned near the $|5/2,5/2\rangle \rightarrow |3/2,3/2\rangle$ and $|5/2,3/2\rangle \rightarrow |3/2,1/2\rangle$ transitions. The relaxation and decoherence rates γ_1, γ_{d1} γ_2 and γ_{d2} are assumed for the addressed transitions. (b) The case of two doping sites. The blue group of thorium nuclei is influenced by a different environment than the yellow one which experiences the additional detunings δ_1 and δ_2 as a function of the magnetic field. See text for further explanations.

We numerically solve Eq. (18) with the initial condition that the hyperfine levels of the lower state are equally populated, i.e., $\rho_{33}(0,z) = 0.5$, $\rho_{44}(0,z) = 0.5$ and with the initial and boundary conditions on the probe field given by Eq. (7). We consider the decoherence rates of $\gamma_{d1} = 2\pi \times 84$ Hz and $\gamma_{d2} = 2\pi \times 251$ Hz which have been estimated for these transitions in ^{229}Th:CaF$_2$ [23].

For an incident probe field of Rabi frequency $10^6\Gamma_0$ detuned to the transition $|2\rangle \rightarrow |4\rangle$ and $|1\rangle \rightarrow |3\rangle$ by $\Delta_2 = -\Delta_1 = 10^9\Gamma_0$ respectively, we obtain the scattered NFS intensity as shown by the thin (black) curve with shading (yellow) in Fig. 13. The signal shows quantum beat features with a frequency of the order of $10^9\Gamma_0$. The origin of this beating is attributed to the intranuclei quantum interference between the two transition pathways the probe field interacts with. The envelope of the beating is seen to be governed by the largest of the two decoherence rates involved, i.e., by $e^{-2\gamma_{d2}t}$. Additionally, from the figure we see that the beating gets damped with time.

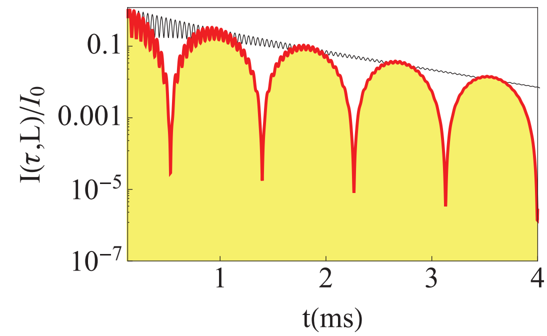

FIG. 13. (Color online) NFS time domain spectra for a multilevel sample with near degenerate transitions. The thin (black) and thick (red) curves with yellow shading are for samples with one and two doping sites, respectively, with laser detuning of $\Delta = 10^9\Gamma_0$. A magnetic-field-dependent detuning of $\delta_i(B) = 10^8\Gamma_0$ in the case of two doping sites is considered. Here, we have considered $\eta_{13}^{(1)} = \eta_{13}^{(2)} = \eta_{13}/2 \simeq 227$ Hz/cm and $\eta_{24}^{(1)} = \eta_{24}^{(2)} = \eta_{24}/2 \simeq 137$ Hz/cm for $\xi \simeq 10^6$. The spontaneous decay rates of the relevant transitions are, respectively, $\gamma_1 = 0.899\Gamma_0$ and $\gamma_2 = 0.533\Gamma_0$. The probe pulse has a duration of $\tau = 0.01$ ms with a Gaussian shape centered on $t_0 = 0.1$ ms.

E. Different doping sites

For the case of two different doping sites we assume that the VUV crystal now comprises of two groups of dopant nuclei represented by the blue and yellow dots in Fig. 12. Thus the index α on the density operator in Eqs. (3)–(5) takes the values 1 and 2 for the two groups. The effect of environmental perturbation on the coherences is included via the decoherence matrix (17) for each group of nuclei. The nuclei of the second group have an additional shift $\delta_k(B)$ $(k = 1, 2)$ of the isomeric level as shown in Fig. 12(b). In the Hamiltonian description in Eq. (2) of the four level system the detunings will now be replaced by $\Delta_1 \rightarrow \Delta_1 + \delta_1(B)$ and $\Delta_2 \rightarrow \Delta_2 + \delta_2(B)$, respectively. As the probe VUV pulse will now simultaneously interrogate the nuclei in both crystal unit cell sites, the field equation will have contributions from the coherences related to both nuclear sites as well as from both transitions of each group. The field equation thus involves several coherences in this case and takes the form

$$\partial_z\Omega_p + \frac{1}{c}\partial_t\Omega_p = i\big[a_{13}\big(\eta_{13}^{(1)}\rho_{13}^{(1)} + \eta_{13}^{(2)}\rho_{13}^{(2)}\big) + a_{24}\big(\eta_{24}^{(1)}\rho_{24}^{(1)} + \eta_{24}^{(2)}\rho_{24}^{(2)}\big)\big], \quad (19)$$

where $\rho^{(1)}$ and $\rho^{(2)}$ are the density matrices for the first and second doping sites, respectively. The dynamics of the coherences from each group are governed by Eq. (4) with the

Hamiltonian containing the modified detuning for the second group.

As before, the probe pulse is assumed to be positively and negatively detuned to the transition $|2\rangle \rightarrow |4\rangle$ and $|1\rangle \rightarrow |3\rangle$ by $10^9\Gamma_0$ in the first group of nuclei. We furthermore assume that the nuclei in the second doping site have an additional hyperfine shift of the levels by $\delta_k(B) = 10^8\Gamma_0\,(k = 1, 2)$ which corresponds to a magnetic field of about 100 gauss. Thus, the nuclei in the second doping site have a laser detuning of $(10^8 - 10^9)\Gamma_0$ for the $|1\rangle \rightarrow |3\rangle$ transition and $(10^9 + 10^8)\Gamma_0$ for the $|2\rangle \rightarrow |4\rangle$ transition. The other parameters of the probe field are the same as in the previously studied case. For computational purpose we consider equal doping of the two groups of nuclei such that $\eta_{13}^{(1)} = \eta_{13}^{(2)}$ and $\eta_{24}^{(1)} = \eta_{24}^{(2)}$.

The NFS time spectrum evaluated numerically by means of Eq. (19) and the respective Bloch equations is shown by the solid (red) curve in Fig. 13. We find a signature of intra- and internuclei quantum interference in the NFS signal. From Fig. 13 we find that the intranuclei quantum interference which leads to beats of order $\Delta_{1,2}$, owing to the two transition pathways in each nucleus, is modulated by internuclei quantum interference of beat frequency $\sim\delta_k(B)$. The origin of internuclei quantum interference is the different hyperfine splitting of the two groups of nuclei. Similar to the uniform doping case here we again see that the envelope of the combined beating pattern is governed by the largest decoherence rate of the system.

V. CONCLUSION

We have carried out an extensive theoretical study of NFS time spectra from a multilevel nuclear ensemble of ^{229}Th doped in a VUV-transparent crystal. Explicit results for three- and four-level configurations interacting with one and two optical fields were presented. In the three-level case we have considered two different configurations, namely the Λ and V-level schemes interacting with two different VUV fields. We have shown that interference effects occurring in such configurations offer signatures of the isomer excitation advantageous for the more precise experimental determination of the transition energy. Our study shows that it is possible to coherently manipulate the signature of the quantum interference in the NFS signal by externally tuning the laser intensity and detuning. Furthermore, the possibility of population trapping in the isomeric state has been investigated. This can be utilized towards controlled subradiance generation in such nuclear isomers thereby opening a new direction in quantum optical manipulation of collective phenomena in nuclear systems. Our study theoretically sustains the concept of nuclear coherent control and paves the way for further nuclear quantum optics applications with ^{229}Th.

ACKNOWLEDGMENT

The authors would like to thank W.-T. Liao for fruitful discussions.

[1] B. R. Beck, C. Y. Wu, P. Beiersdorfer, G. V. Brown, J. A. Becker, K. J. Moody, J. B. Wilhelmy, F. S. Porter, C. A. Kilbourne, and R. L. Kelley, LLNL-PROC-415170 (2009); B. R. Beck, J. A. Becker, P. Beiersdorfer, G. V. Brown, K. J. Moody, J. B. Wilhelmy, F. S. Porter, C. A. Kilbourne, and R. L. Kelley, Phys. Rev. Lett. **98**, 142501 (2007).

[2] T. J. Bürvenich, J. Evers, and C. H. Keitel, Phys. Rev. Lett. **96**, 142501 (2006).

[3] A. Pálffy, J. Evers, and C. H. Keitel, Phys. Rev. C **77**, 044602 (2008).

[4] W.-T. Liao, A. Pálffy, and C. H. Keitel, Phys. Lett. B **705**, 134 (2011).

[5] M. O. Scully and M. S. Zubairy, *Quantum Optics* (Cambridge University Press, Cambridge, England, 1997).

[6] Z. Ficek and S. Swain, *Quantum Interference and Coherence* (Springer, Berlin, 2005).

[7] S. P. Tewari and G. S. Agarwal, Phys. Rev. Lett. **56**, 1811 (1986).

[8] S. E. Harris, J. E. Field, and A. Imamoğlu, Phys. Rev. Lett. **64**, 1107 (1990).

[9] K.-J. Boller, A. Imamoğlu, and S. E. Harris, Phys. Rev. Lett. **66**, 2593 (1991).

[10] E. Arimondo, Prog. Opt. **35**, 257 (1996).

[11] K. Bergmann, H. Theuer, and B. W. Shore, Rev. Mod. Phys. **70**, 1003 (1998).

[12] O. Kocharovskaya and Ya. I. Khanin, Pis'ma Zh. Eksp. Teor. Fiz. **48**, 581 (1988) [JETP Lett. **48**, 630 (1988)].

[13] M. O. Scully, S. Y. Zhu, and A. Gavrielides, Phys. Rev. Lett. **62**, 2813 (1989).

[14] M. Jain, H. Xia, G. Y. Yin, A. J. Merriam, and S. E. Harris, Phys. Rev. Lett. **77**, 4326 (1996).

[15] M. Gross and S. Haroche, Phys. Rep. **93**, 301 (1982).

[16] M. Macovei, J. Evers, and C. H. Keitel, Phys. Rev. Lett. **91**, 233601 (2003); Phys. Rev. A **71**, 033802 (2005).

[17] S. Das, G. S. Agarwal, and M. O. Scully, Phys. Rev. Lett. **101**, 153601 (2008).

[18] S. Das, A. Rakshit, and B. Deb, Phys. Rev. A **85**, 011401(R) (2012).

[19] G. C. Baldwin, J. P. Neissel, J. Terhune, and L. Tonks, Proc. IEEE **51**, 1247 (1963).

[20] D. Marcuse, Proc. IEEE **51**, 849 (1963).

[21] S. Matinyan, Phys. Rep. **298**, 199 (1998).

[22] E. Peik and C. Tamm, Europhys. Lett. **61**, 181 (2003).

[23] G. A. Kazakov, A. N. Litvinov, V. I. Romanenko, L. P. Yatsenko, A. V. Romanenko, M. Schreitl, G. Winkler, and T. Schumm, New J. Phys. **14**, 083019 (2012).

[24] V. V. Flambaum, Phys. Rev. Lett. **97**, 092502 (2006).

[25] E. V. Tkalya, Phys. Rev. Lett. **106**, 162501 (2011).

[26] O. Kocharovskaya, R. Kolesov, and Y. Rostovtsev, Phys. Rev. Lett. **82**, 3593 (1999).

[27] W.-T. Liao, A. Pálffy, and C. H. Keitel, Phys. Rev. Lett. **109**, 197403 (2012).

[28] B. Adams, C. Buth, S. M. Cavaletto, J. Evers, Z. Harman, C. H. Keitel, A. Pálffy, A. Picón, R. Röhlsberger, Y. Rostovtsev, and K. Tamasaku, J. Mod. Opt. **60**, 2 (2013).

[29] W.-T. Liao, A. Pálffy, and C. H. Keitel, Phys. Rev. C **87**, 054609 (2013).

[30] J. P. Hannon and G. T. Tramell, in *Resonant Anomalous Xray Scattering*, edited by C. J. S. G. Materlik and K. Fisher (North-Holland, Amsterdam, 1994).

[31] A. M. Afanas'ev and Y. Kagan, Pis'ma Zh. Eksp. Teor. Fiz. **2**, 130 (1965) [JETP Lett. **2**, 81 (1965)].

[32] J. P. Hannon and G. T. Tramell, Hyperfine Interact. **123/124**, 127 (1999).
[33] R. Röhlsberger, *Nuclear Condensed Matter Physics with Synchrotron Radiation: Basic Principles, Methodology and Applications* (Springer, Berlin, 2004).
[34] *Nonlinear Optics, Quantum Optics, and Ultrafast Phenomena with X-Rays*, edited by B. Adams (Springer, Berlin, 2003).
[35] Yu. V. Shvyd'ko *et al.*, Phys. Rev. B **57**, 3552 (1998).
[36] W-T. Liao, S. Das, C. H. Keitel, and A. Pálffy, Phys. Rev. Lett. **109**, 262502 (2012).
[37] W. G. Rellergert, D. DeMille, R. R. Greco, M. P. Hehlen, J. R. Torgerson, and E. R. Hudson, Phys. Rev. Lett. **104**, 200802 (2010); W. G. Rellergert, S. T. Sullivan, D. DeMille, R. R. Greco, M. P. Hehlen, R. A. Jackson, J. R. Torgerson, and E. R. Hudson, IOP Conf. Ser.: Mater. Sci. Eng. **15**, 012005 (2010).
[38] MOTIF.23, a program for fitting time spectra of nuclear resonant forward scattering, available from the anonymous ftp://i2aix04.desy.de/pub/motif/
[39] S. G. Porsev, V. V. Flambaum, E. Peik, and C. Tamm, Phys. Rev. Lett. **105**, 182501 (2010).
[40] X. Zhao, Y. N. Martinez de Escobar, R. Rundberg, E. M. Bond, A. Moody, and D. J. Vieira, Phys. Rev. Lett. **109**, 160801 (2012).
[41] A. Pálffy, W. Scheid, and Z. Harman, Phys. Rev. A **73**, 012715 (2006); F. F. Karpeshin and M. B. Trzhaskovskaya, Phys. Rev. C **76**, 054313 (2007); A. Pálffy, Contemp. Phys. **51**, 471 (2010); S. K. Arigapudi and A. Pálffy, Phys. Rev. A **85**, 012710 (2012).
[42] G. V. Smirnov, Hyperfine Interact. **97/98**, 551 (1996).
[43] U. van Bürck, Hyperfine Interact. **123/124**, 483 (1999).
[44] Y. Kagan, Hyperfine Interact. **123/124**, 83 (1999).
[45] R. Irrgang, M. Drescher, F. Gierschner, M. Spieweck, and U. Heinzmann, Meas. Sci. Technol. **9**, 422 (1998).
[46] R. J. Jones, K. D. Moll, M. J. Thorpe, and J. Ye, Phys. Rev. Lett. **94**, 193201 (2005).
[47] A. Ozawa, J. Rauschenberger, Ch. Gohle, M. Herrmann, D. R. Walker, V. Pervak, A. Fernandez, R. Graf, A. Apolonski, R. Holzwarth, F. Krausz, T. W. Hänsch, and Th. Udem, Phys. Rev. Lett. **100**, 253901 (2008).
[48] M. O. Scully, Laser Phys. **17**, 635 (2007); Phys. Rev. Lett. **102**, 143601 (2009).
[49] R. Röhlsberger, K. Schlage, B. Sahoo, S. Couet, and R. Rüffer, Science **328**, 1248 (2010).
[50] A. Pálffy, C. H. Keitel, and J. Evers, Phys. Rev. Lett. **103**, 017401 (2009).
[51] A. Pálffy and J. Evers, J. Mod. Opt. **57**, 1993 (2010).
[52] M. D. Crisp, Phys. Rev. A **1**, 1604 (1970).
[53] Y. Kagan, A. M. Afanas'ev, and V. G. Kohn, J. Phys. C **12**, 615 (1979).
[54] A. Junker, A. Pálffy, and C. H. Keitel, New J. Phys. **14**, 085025 (2012).
[55] C. Cohen-Tannoudji, G. Grynberg, and J. Dupont-Roc, *Atom-Photon Interactions* (Wiley-VCH Verlag, Berlin, 1997).
[56] Yu. V. Shvydko and U. van Bürck, Hyperfine Interact. **123/124**, 511 (1999).
[57] S. H. Autler and C. H. Townes, Phys. Rev. **100**, 703 (1955); T. E. Glover, M. P. Hertlein, S. H. Southworth, T. K. Allison, J. van Tilborg, E. P. Kanter, B. Krässig, H. R. Varma, B. Rude, R. Santra, A. Belkacem, and L. Young, Nat. Phys. **6**, 69 (2009).
[58] C. Chen, Z. Xu, D. Deng, J. Zhang, G. K. L. Wong, B. Wu, N. Ye, and D. Tang, Appl. Phys. Lett. **68**, 2930 (1996); C. T. Chen, G. L. Wang, X. Y. Wang, and Z. Y. Xu, Appl. Phys. B **97**, 9 (2009).
[59] T. Togashi, T. Kanai, T. Sekikawa, S. Watanabe, C. Chen, C. Zhang, Z. Xu, and J. Wang, Opt. Lett. **28**, 254 (2003).
[60] Y. Nomura, Y. Ito, A. Ozawa, X. Wang, C. Chen, S. Shin, S. Watanabe, and Y. Kobayashi, Opt. Lett. **36**, 1758 (2011).
[61] J. Nolting, H. Kunze, I. Schütz, and R. Wallenstein, Appl. Phys. B **50**, 331 (1990).
[62] D. Sun, Z. E. Sariyanni, S. Das, and Y. V. Rostovtsev, Phys. Rev. A **83**, 063815 (2011).
[63] G. S. Agarwal, *Springer Tracts in Modern Physics: Quantum Optics* (Springer-Verlag, Berlin, 1974).
[64] M. Kiffner, M. Macovei, J. Evers, and C. H. Keitel, Prog. Opt. **55**, 85 (2010).
[65] M. O. Scully, Phys. Rev. Lett. **104**, 207701 (2010).
[66] K. E. Dorfman, P. K. Jha, and S. Das, Phys. Rev. A **84**, 053803 (2011).
[67] T. Bienaimé, N. Piovella, and R. Kaiser, Phys. Rev. Lett. **108**, 123602 (2012).